Supplementary Materials for

Rocket Launcher Mechanism of Collaborative Actin Assembly Defined by Single-Molecule Imaging

Dennis Breitsprecher, Richa Jaiswal, Jeffrey P. Bombardier, Christopher J. Gould, Jeff Gelles,* Bruce L. Goode*

*To whom correspondence should be addressed. E-mail: goode@brandeis.edu (B.L.G.); gelles@brandeis.edu (J.G.)

Published 1 June 2012, *Science* **336**, 1164 (2012)
DOI: 10.1126/science.1218062

This PDF file includes:

Other Supplementary Material for this manuscript includes the following:
(available at www.sciencemag.org/cgi/content/full/336/6085/1164/DC1)

Supporting Online Material

Rocket launcher mechanism of collaborative actin assembly defined by single-molecule imaging

Dennis Breitsprecher[1], Richa Jaiswal[1], Jeffrey P. Bombardier[2], Christopher J. Gould[1], Jeff Gelles[2]*, and Bruce L. Goode[1]*

[1]Department of Biology, Brandeis University, Waltham, MA 02454

[2]Department of Biochemistry, Brandeis University, Waltham, MA 02454

*To whom correspondence should be addressed: goode@brandeis.edu (B.L.G.), gelles@brandeis.edu (J.G.)

This PDF file includes

Materials and Methods

Figures S1 to S13

Supplementary Movie Legends

Material and methods

Constructs

Expression plasmids for mDia1-C *(21)*, mDia1-FH1FH2 (*22*), APC-C (*15, 23*), CapZ (*23*), and human profilin (*11*) have been described previously. SNAP-tags allow highly specific labeling with benzylguanine-fluorophore adducts (*24*). For expression of SNAP-mDia1-C in yeast, the SNAP coding region was PCR amplified from the SNAP-tag-T7-2-vector (NEB, Ipswitch, MA) but with a C-terminal GGSGGS flexible linker, and subcloned into BglII/BamHI sites of the URA3 6xHis GAL1/10 yeast-expression plasmid pJM45 (Moseley et al., 2004). mDia1-C was subcloned into the BamH1/Not1 sites of this vector (pCG105). For expression of SNAP-APC-C, the SNAP coding gene was PCR amplified from the SNAP-tag-T7-2-vector (NEB) but with a C-terminal GGSGGS flexible linker, and subcloned into BamHI/EcoRI sites of the pGex-6P1-Vector (GE Healthcare, Piscataway, NJ). The insert APC-C-6xHis was subcloned from a previously described plasmid (*15*) and introduced into the EcoRI/NotI sites of the plasmid above, yielding a vector expressing GST-SNAP-APC-C-6xHis.

Protein purification

Unlabeled rabbit-muscle actin, pyrenyliodoacetamide-labeled actin (pyrene actin), and Oregon-Green-labeled actin were purified as described (*11, 25, 26*). Biotinylated actin was prepared by rapidly mixing 1 mL of actin (150 µM) in 5 mM Hepes pH 7.3, 0.2 mM CaCl2, 0.5 mM DTT and 0.2 mM ATP with 20 µl a 70 mM NHS-XX-Biotin (Merck KGaA, Darmstadt, Germany) solution in anhydrous DMF. After incubating the mixture for 1 hr at room temperature, free NHS-XX-Biotin was removed by gel filtration on a Superose12 10/30 column (GE Healthcare, Piscataway, NJ). CapZ and human profilin were purified as described (*27*). 6xHis-tagged mDia1-C and mDia1-FH1FH2 were purified from *S. cerevisiae* as described (*22*). 6xHis-tagged SNAP-549-mDia1-C was prepared as described with minor modifications (*21*). Briefly, plasmids were transformed into yeast strain BJ2168 and 2 liters of cells were grown at 25°C to late log phase (OD_{600} = 0.8) in selective medium containing 2% raffinose. Galactose (2% final) was added to induce expression for 12-16 hr. Yeast cells were harvested by centrifugation and resuspended in a 3:1 (v/w) ratio of water, mechanically lysed in a Retsch Mixer Mill (MM200) (Retsch Inc., Newton, PA) at liquid N_2 temperature, and stored at -80°C. To initiate protein purification, 10 g of frozen yeast powder was thawed at 1:3 (w/v) of 20 mM imidazole (pH 8.0), 1.5X PBS (40 mM

sodium phosphate buffer, 200 mM NaCl, pH 7.4), 0.5% Nonidet P-40, 1 mM DTT, and protease inhibitors (final 1 mM phenylmethylsulfonyl fluoride and 0.5 µg/ml each of antipain, leupeptin, pepstatinA, chymostatin, and aprotinin). 50 ml of this yeast lysate was centrifuged for 80 min at 60,000 rpm, 4°C in a Ti70 rotor (Beckman/Coulter, Fullerton, CA). The supernatant was rotated with 0.75 ml of Ni^{2+}-NTA-agarose beads (Qiagen, Valencia, CA) and 20 µM SNAP-surface 549 (NEB, Ipswitch, MA) at 4°C overnight. To remove free dye, beads were washed three times with 20 mM imidazole (pH 8.0), 1X PBS, 1 mM DTT, 200 mM NaCl. Labeled SNAP-549-mDia1-C was eluted with 0.5 ml of 300 mM imidazole pH 8.0, 50 mM Tris pH 8.0, 100 mM NaCl, 1 mM DTT, 5% glycerol, then purified by gel filtration on a Superose 6 column (GE Healthcare) equilibrated in formin buffer (20 mM Hepes (pH 7.5), 1 mM EDTA, 150 mM KCl, 5% glycerol).

APC-C (Dual-tagged with N-terminal GST, C-terminal 6xHis) was purified from *E. coli* by sequential steps using Ni-NTA and glutathione-agarose beads as described (*15*). SNAP-APC-C was purified similarly from *E. coli*, but with an additional labeling step introduced. Glutathione-agarose-bound SNAP-APC-C was labeled overnight at 4°C using 50 µM dye (SNAP-surface647; NEB). To remove free dye, beads were washed three times in 500 µl of 20 mM Tris-Cl^- (pH 7.5), 600 mM KCl, 0.5 mM DTT, and 5% glycerol. Labeled SNAP-647-APC-C was eluted with the same buffer containing 30 mM glutathione, then purified by gel filtration on a Superose 6 column (GE Healthcare) equilibrated in the same buffer lacking glutathione. The peak fractions were pooled, dialyzed into storage buffer (same as above except with KCl reduced to 300 mM), aliquoted, snap-frozen in liquid N_2, and stored at -80°C.

Concentrations of SNAP-tagged proteins and degree of labeling were determined by densitometry of Coomasie-stained bands on SDS-PAGE gels compared to BSA standards, and by measuring fluorophore absorbance in solution using the extinction coefficients: SNAP-surface549: ε_{560} = 140,300 M^{-1} cm^{-1}; SNAP-surface647: ε_{650} = 240,000 M^{-1} cm^{-1}. The concentration and degree of labeling of OG-actin was determined as described (*28*).

Pyrene-actin assembly assays

Monomeric actin (2 µM; 5% pyrene labeled) in G-buffer (10 mM Tris-Cl^- pH 8.0, 0.2 mM ATP, 0.2 mM $CaCl_2$, and 0.2 mM DTT) was converted to Mg-ATP-actin immediately before each reaction (*21*). Actin was mixed with proteins or control buffer and 3 µl of 20X initiation mix (IM)

(40 mM $MgCl_2$, 10 mM ATP, 1 M KCl). Pyrene fluorescence was monitored over time at excitation 365 nm and emission 407 nm at 25°C in a fluorimeter (Photon Technology International, Lawrenceville, NJ).

For pointed end elongation assays, Pyrene fluorescence was monitored over time at excitation 365 nm and emission 407 nm at 25°C in a fluorescence multi-well plate reader (Tecan Group Ltd, Männedorf, Switzerland). Gelsolin-F-actin seeds were prepared by polymerizing 10 µM G-actin in 1X IM in the presence of 130 nM gelsolin overnight at 4°C. Gelsolin-F-actin seeds were then added to a solution containing 2.5 nM CapZ and APC-C in 1.25X IM to reach a final concentration of 250 nM F-actin and 3.25 nM gelsolin. 80 µl of this solution was added to 20 µl 12 µM G-actin (10% pyrene labeled) in G-buffer to initiate polymerization. As a control experiment to test whether filament polymerization occured exclusively from pointed ends, 5 µM profilin was added instead of APC-C to inhibit pointed end elongation.

TIRF microscopy

Glass coverslips (18 × 18 mm #1.5, Fisher Scientific, Pittsburg, PA) were sonicated for 1 hr in H_2O with 1% Versaclean detergent (Fisher Scientific, Pittsburg, PA), followed by 15 min sonications in 1M HCl and in 1M KOH, respectively. Next, coverslips were sonicated in ethanol for >1 hr, rinsed extensively with 60°C H_2O, and dried in a N_2 stream. The cleaned coverslips were stored for up to 1 month. Prior to TIRF experiments, each coverslip was rinsed with H_2O, dried with N_2, and then derivatized by applying 100 µl of 2 mg/ml mPEG-silane MW 2,000 and 2 µg/ml biotin-PEG-silane MW 3,400 (both from Laysan Bio, Arab, AL) in 80% ethanol brought to pH 2.0 with HCl, and then dried by baking at 70°C for 16 hr. The coverslips were rinsed extensively with ddH_2O and dried in an N_2-stream before use.

Flow cells were assembled by placing 4 parallel strips of double sided tape (2.5 cm × 2 mm × 120 µm) onto an ethanol washed glass slide (25 × 75 mm) with ~3 mm spacing between the strips. A PEG-coated coverslip was then positioned over the strips of double-sided tape, producing three separate flow chambers per slide.

TIRFM was performed using a Nikon-Ti2000 inverted microscope equipped with a 150 mW Ar^+ laser (emission 488 nm), and two HeNe lasers (15 mW, emission 633 nm, and 5 mW, emission 543 nm; all three lasers from Mellot Griot, Carlsbad, CA; all three operated at maximum power in all experiments), a CFI Apo TIRF 60x H objective (Nikon Instruments Inc., New York, NY), and an cooled, back-illuminated EMCCD camera with a pixel size of 0.27 µm (Andor Ixon, Belfast, Northern Ireland). The EM gain of the camera was set to 300 for all experiments. During measurements, focus was maintained by the Perfect Focus system (Nikon Instruments Inc., New York, NY). Illumination times were regulated by the shutter controller Lambda SC (Sutter Instrument, Novato, CA). For multicolor experiments in which actin polymerization was observed, we cyclically imaged SNAP-549-Dia1-C (1 frame, 500 ms, 543 nm excitation), OG actin (1 frame, 50 ms, 488 nm excitation) and SNAP-647-APC-C (1 frame; 200 ms, 633 nm excitation). Cycle times ranged from 3-15 s. A separate, single-fluor filter cube was used for each color. Image acquisition was controlled by NIS-Elements software (Nikon Instruments Inc., New York, NY).

Prior to each reaction, flow cells were incubated with PBS + 1% BSA for 2 min, then with 20 mM Tris-Cl^- (pH 8.0), 1 mM DTT, 100 mM KCl, 4 µg/mL streptavidin for 15 sec, followed by washing with 50 µl PBS + 1% BSA. The flow cell was then equilibrated with TIRF buffer [10 mM imidazole (pH 7.4), 50 mM KCl, 1 mM $MgCl_2$, 1 mM EGTA, 0.2 mM ATP, 10 mM DTT, 15 mM glucose, 20 µg/ml catalase, 100 µg/ml glucose oxidase, and 0.5% methylcellulose (4000 cP)]. For monitoring actin polymerization, actin regulatory proteins were diluted into TIRF buffer, then rapidly mixed with 1 µM actin (10% OG-labeled and 0.2% biotinylated) and introduced into the flow cell, which was then mounted on the microscope stage for imaging. The time between initial mixing of the proteins and the start of TIRFM recording was typically 45-60 sec. Filament elongation rates were determined as described (*29*). Since concentrations of APC-C >10 nM displayed bundling activity, analysis of elongation rates in those reactions was limited to non-bundled single filaments. Reported errors on elongation rates reflect SE of pooled data from at least two independent experiments.

For single-molecule bleaching experiments on SNAP-647-APC-C or SNAP-549-mDia1-C, a solution containing 1 nM of the protein (in TIRF buffer without glucose oxidase and catalase) was transferred into a flow cell as above, and immobile spots (passively absorbed to the cover

slip surface) were subjected to continuous illumination and imaged every 0.5 seconds. For dual-color bleaching experiments on SNAP-647-APC-C/SNAP-549-mDia1-C complexes, 200 nM of each of the proteins were pre-incubated together for 30 min in TIRF buffer (in presence or absence of 20 µM actin monomers previously incubated for 30 min with a 10-fold molar excess of LatB), and diluted into TIRF buffer to 1 nM each prior to imaging. Samples were alternately exposed to the two excitation wavelengths for 0.5 s each. For triple-color visualization of SNAP-647-APC-C/SNAP-549-mDia1-C/OG-actin complexes, 200 nM of the SNAP-proteins were pre-incubated for 30 min with 8 µM OG-actin monomers (previously incubated for 30 min with a 10-fold molar excess of LatB) and, if stated, 8 µM profilin, diluted to a final concentration of 1 nM for the SNAP-proteins, respectively, and 40 nM LatB-OG-actin (and 40 nM profilin), and alternately exposed to the three excitation wavelengths for 0.5 s each. Experiments with a 50-fold excess of profilin were conducted equivalently, with the exception that proteins were diluted into TIRF-buffer containing 1.96 µM profilin. For the colocalization experiments in Fig. 2A and C, a control analyses were performed in which we overlaid images of SNAP-549-mDia-C and SNAP-647-APC-C from two unrelated fields of view and measured the extent of apparent colocalization seen as overlap of the spots in these uncorrelated images.

Acquired image sequences were converted to 16 bit TIFF files with ImageJ (http://imagej.nih.gov/ij/) using the 'NIS to ImageJ' plugin (Nikon Instruments Inc., New York, NY). Background fluorescence was subtracted automatically using the background subtraction tool (rolling ball radius 20 pixel) implemented in the ImageJ software. Fluorescence intensities of spots were obtained by measuring the integrated fluorescence signal from a small region of interest (edge length 4 pixels) that tracked the spot over time to compensate for stage drift.

To measure single molecule bleaching events, video recordings were first filtered by a sliding window average (width 2 frames) to reduce background noise. Then, stepwise reductions in the integrated fluorescence intensity time records of individual spots were subjectively identified and counted.

In experiments in which actin filaments were present, the glucose oxidase/glucose oxygen scavenger was found to be essential to prevent filament disassembly due to photodamage. Under these conditions, SNAP-647-APC-C was highly photostable and it therefore was impractical to

use photobleaching to measure the number of fluorescent SNAP-647-APC-C subunits present in a spot. Instead, we determined the fluorescent subunit count by comparing the spot fluorescence intensity to the average size of the comparatively rare step photobleaching events (~25 to 40 events per 138 × 138 μm field of view) observed in the same sample. The same approach was used to count the number of SNAP-549-mDia1-C subunits present in APC-C/mDia1 in the absence of oxygen scavenger.

For determination of protein oligomeric state by single molecule fluorescence, the measured distribution of fluorescence intensity or distribution of numbers of photobleaching steps was compared to the probability distribution $p(i)$ of the number of fluorescent subunits i predicted for a protein oligomer consisting of n monomers, as calculated from the binomial distribution based on the measured subunit labeling stoichiometry s, as

$$p(i) = \left(\frac{n!}{i!(n-i)!} \right) s^i (1-s)^{n-i}.$$

This approach is expected to be valid because SNAP-tagged protein monomers each have only a single site for reaction with the benzylguanine-dye adduct. Consistent with this, measured values of s were always <1.

Supporting figures

Fig. S1

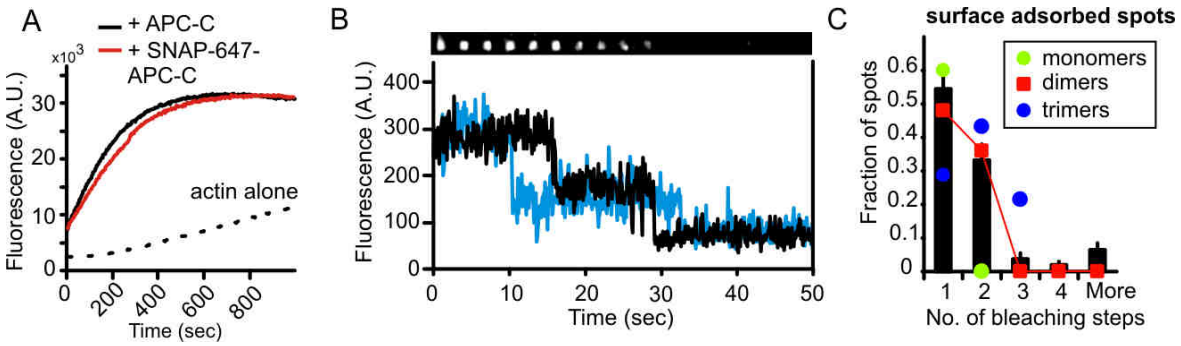

Fig. S1: Activity and Multimerization of SNAP-647-APC-C. (A) Actin assembly assay (2 µM, 5% pyrene-labeled) in the presence of APC-C or SNAP-647-APC-C. (B) Stepwise photobleaching of surface-adsorbed SNAP-647-APC-C spots (bottom: two examples in graph, black and blue). Time-lapse micrographs of a single SNAP-647-APC-C spot (top), corresponding to the black trace. (C) Distribution of number of photobleaching steps per SNAP-647-APC-C spot (bars ± SE; $n = 156$), and distributions predicted for different oligomeric states (see symbols) given the independently measured labeling stoichiometry (0.6 dye per monomer).

Fig. S2

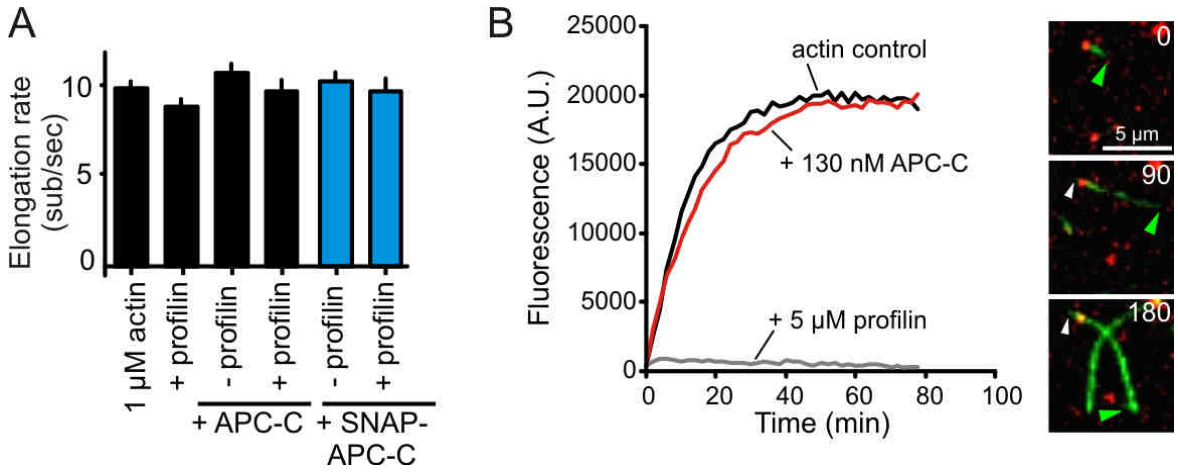

Fig. S2: Elongation of actin filament ends in the presence of APC-C-constructs. (A) Filament barbed end elongation rates for reactions containing 1 µM OG-actin with and without 10 nM SNAP-647-APC-C or 10 nM APC-C, in presence or absence of 5 µM profilin, as determined by TIRFM. Pooled data from three experiments; bars ± SE; $n > 60$. Elongation rates reactions in presence or absence of profilin are equal within experimental error ($p > 0.06$). (B) (Left) Actin filament pointed end elongation from gelsolin-capped F-actin seeds (200 nM F-actin, 2.5 nM gelsolin) in presence of 2.4 µM pyrene-G-actin (10% labeled) and APC-C (red curve). 2 nM CapZ was added to suppress barbed end elongation from APC-C-nucleated filaments. The black curve shows an actin control, the grey curve shows a negative control reaction containing 5 µM profilin to inhibit pointed end growth. (Right) TIRFM micrograph of the elongation of a SNAP-647-APC-C (red) nucleated actin filament (green). The green arrowhead marks the barbed end, the white arrowhead marks the slow-growing pointed end. Time is indicated in seconds.

Fig. S3

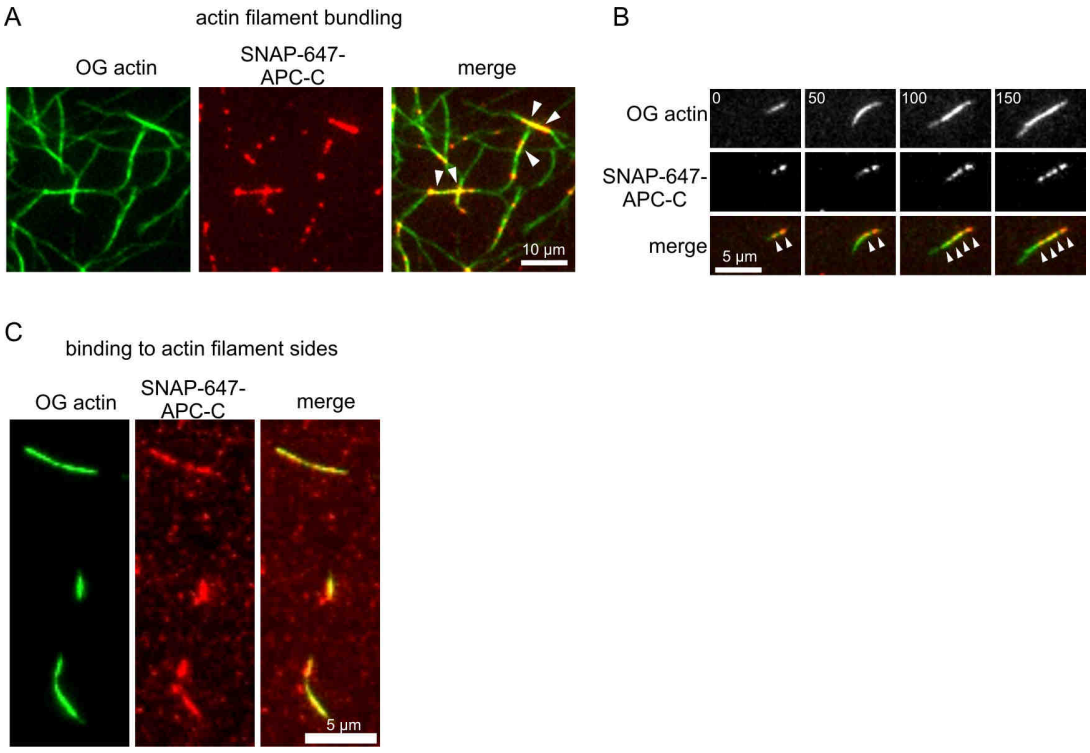

Fig. S3: Higher concentrations of APC-C mediate actin filament bundling. (A) 1 µM OG-actin (10% labeled) was polymerized in the presence of 50 nM SNAP-647-APC-C, resulting in filament bundles decorated by SNAP-647-APC-C (white arrowheads). (B) Time course of SNAP-647-APC-C accumulation on filament sides and concomitant bundling (white arrowheads); experiment conducted as in A. Time indicated in seconds. (C) Filaments preassembled from 1 µM OG-actin (10% labeled) were diluted 10-fold in 1X TIRF buffer containing 50 nM SNAP-647-APC-C and then imaged by TIRFM. Single filaments were decorated by SNAP-647-APC-C.

Fig. S4

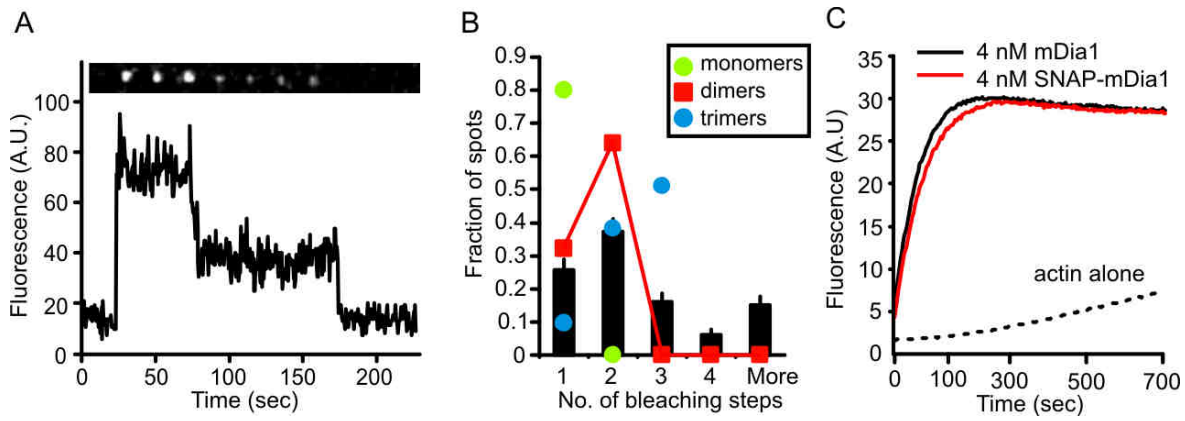

Fig S4: Activity and oligomerization of SNAP-549-mDia1-C. (A) Stepwise photobleaching of surface-adsorbed SNAP-549-mDia1-C. (B) Distribution of number of bleaching events per spot (bars ± SE; n = 226). Predicted distributions for different oligomeric states (symbols) were calculated based on the independently measured labeling stoichiometry (0.79 dye per monomer). (C) Actin assembly (2 µM, 5% pyrene-labeled) in the presence of mDia1-C or SNAP-549-mDia1-C.

Fig. S5

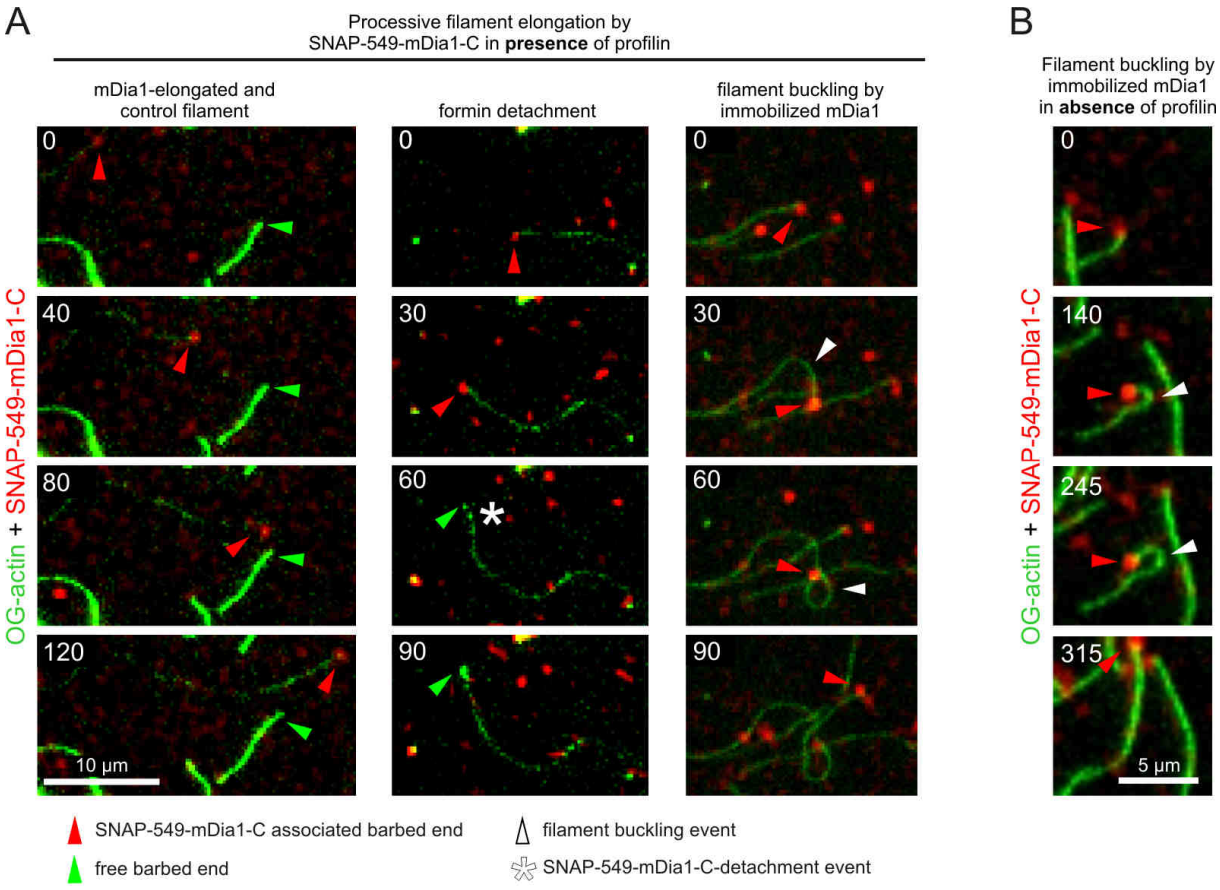

Fig. S5: Processive actin filament elongation by single SNAP-549-mDia1-C molecules in presence and absence of profilin. Conditions as in Figures 1D and E. (A) (Left) Dual-color TIRF micrographs showing a dim, fast-growing, SNAP-549-mDia1-C-elongated filament (red arrowhead) and a bright, slow-growing control filament (green arrowhead) in the same field. (Middle) Occasionally, SNAP-549-mDia1-C (red arrowhead) dissociates (asterisk) from the filament end, resulting in an increase in filament brightness and a decrease in the elongation rate of the free barbed end (green arrowhead). (Right) Filament buckling (white arrowhead) due to transient attachment of SNAP-549-mDia1-C to the slide surface. Note that SNAP-549-mDia1-C detaches and continues to elongate the filament (last frame). (B) Filament buckling (white arrowhead) by surface-attached SNAP-549-mDia1-C (red arrowhead) in the absence of profilin. Time is indicated in seconds. Collectively, these observations argue for a continuous association

of SNAP-549-mDia1-C with the growing filament. Similar behaviors were previously reported for unlabeled formin molecules *(11, 30, 31).*

Fig. S6

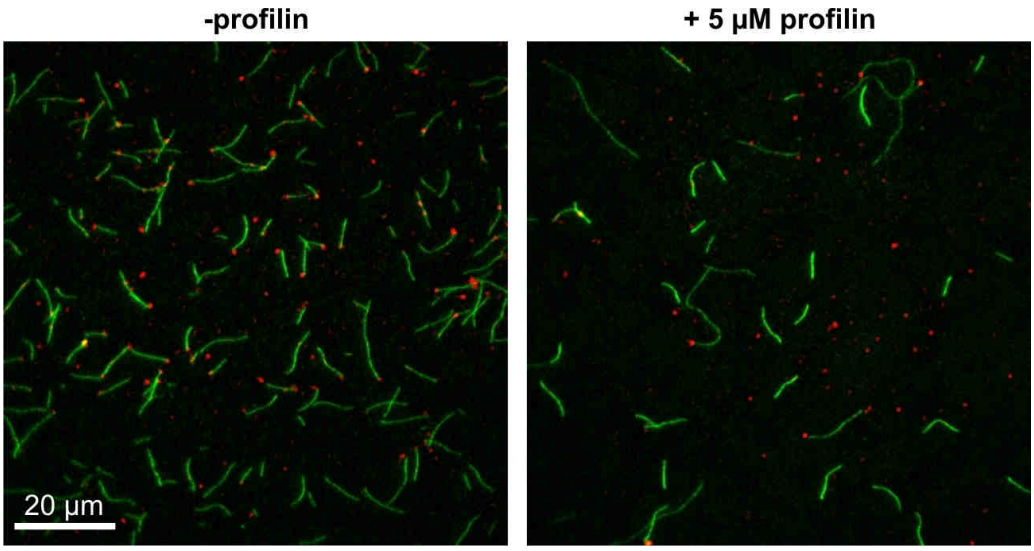

Fig. S6: Low magnification view of SNAP-549-mDia1-C-mediated actin assembly. The micrographs show a 100 × 100 µm field of view of actin assembly reactions containing 50 pM SNAP-549-mDia1-C (red) and 1 µM OG-actin (green) in the presence and absence of profilin. Images were taken 200 seconds after initiation of the reaction. Note the presence of bright filaments without formin molecules on their ends in the reaction containing profilin.

Fig. S7

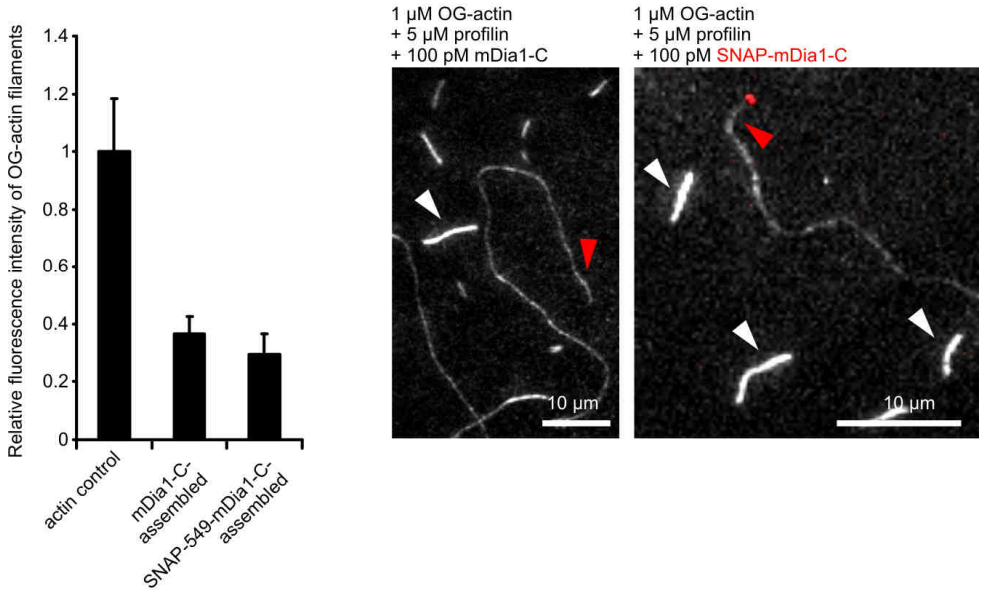

Fig. S7: Decreased fluorescence intensity of mDia1-C-assembled filaments in the presence of profilin. The OG-actin fluorescence intensity of filaments assembled by mDia1-C and SNAP-549-mDia1-C in presence of 5 µM profilin (red arrowheads in micrographs) was quantified and compared to the fluorescence intensity of spontaneously-assembled control filaments in the same reactions (white arrowheads in micrographs), arbitrarily set at 1 in the graph. Error bars represent SD from $n > 30$ filaments.

Fig. S8

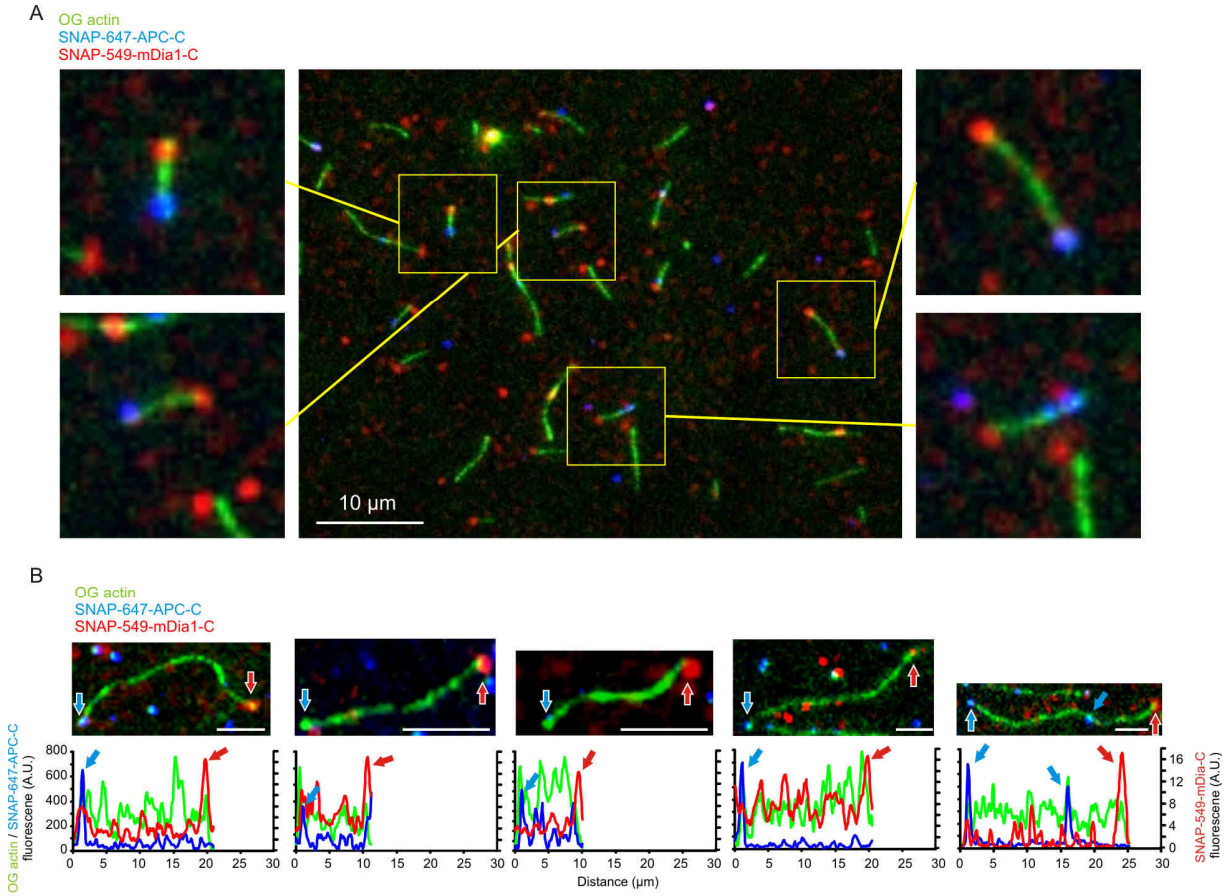

Fig. S8: Actin assembly by SNAP-647-APC-C and SNAP-549-mDia1-C in the presence of CapZ and profilin. (A) Large field of view of a reaction equivalent to that shown in Figure 3A. The micrograph was taken 100 seconds after initiation of actin polymerization. Insets show magnified views of actin filaments (green) with SNAP-647-APC-C fluorescence (blue) near the pointed end and SNAP-549-mDia1-C fluorescence (red) at the barbed end. (B) Five additional examples of filaments assembled by SNAP-647-APC-C and SNAP-549-mDia1-C in presence of 1 nM CapZ and 5 µM profilin, each shown at a single time point. Images (top) and corresponding profiles of fluorescence intensity along the length of the filament (bottom). Arrows mark mDia1 (red), and APC (blue). Note that in one of the examples (rightmost panel), a second SNAP-647-APC-C molecule associates with the side of the filament during polymerization (second blue arrow at 16 µm). Scale bars, 5 µm.

Fig. S9

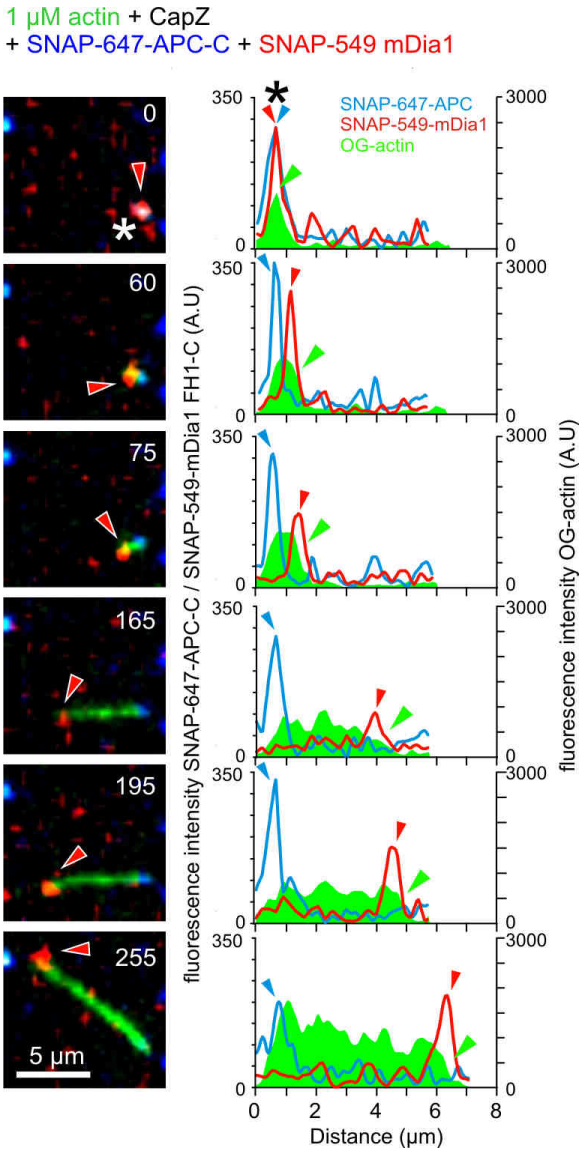

Fig. S9: Actin filament assembly by APC-C and mDia1-C in the presence of CapZ (analogous to Fig. 3A, but in the absence of profilin). Triple-color TIRFM of assembly of 1 µM OG-actin (green) in the presence of 50 pM SNAP-549-mDia1-C (red), 5 nM SNAP-647-APC-C (blue), and 1 nM CapZ. Asterisks indicates APC/mDia1/actin nucleation complex. Images (left; time in seconds) and corresponding profiles of fluorescence intensity along the length of the filament (right). Arrowheads mark barbed end (green), mDia1 (red), and APC (blue).

Fig. S10

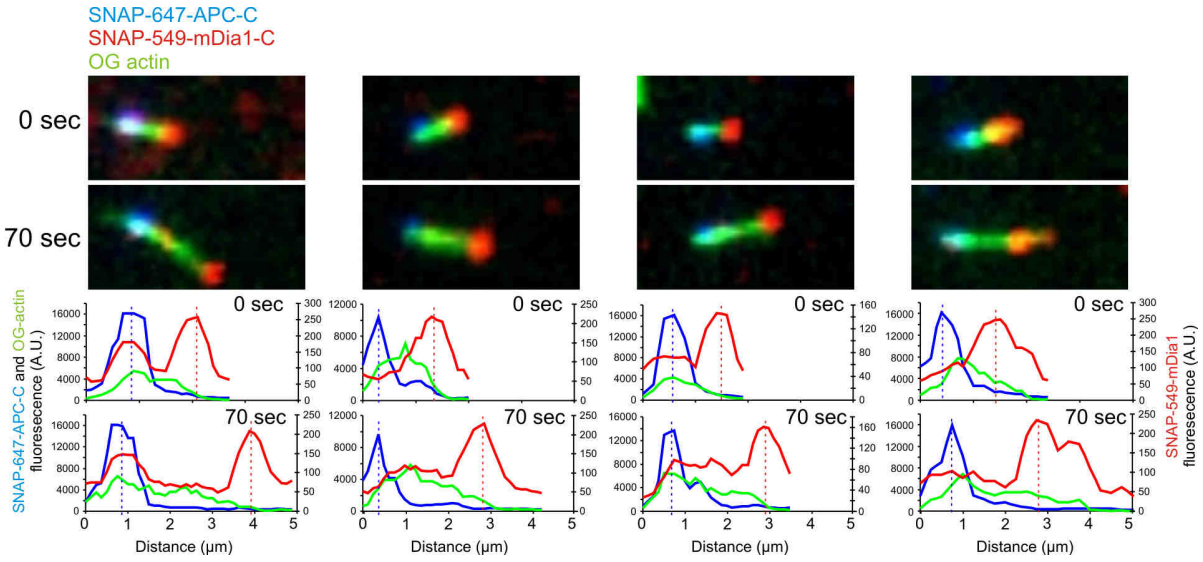

Fig. S10: Examples of SNAP-549-mDia1-C/SNAP-647-APC-C complexes already separated at the onset of image recording. Conditions and plots as in Figure S9. Triple-color TIRFM images showing short actin filaments (green) with SNAP-647-APC-C (blue) at their pointed ends and SNAP-549-mDia1-C at their barbed ends in the presence of 1 nM CapZ (but no profilin). Images are from the first frame of the recording and 70 seconds afterward. Scale bar, 5 µm.

Fig. S11

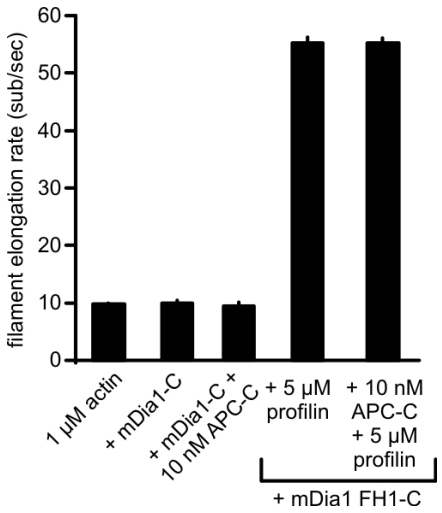

Fig. S11: Actin filament elongation rates in the presence and absence of mDia1-C, APC-C, and/or profilin. Rates determined by TIRFM using 1 µM actin (10% OG-labeled), and 5 µM profilin where indicated. Measurements in the presence of profilin were restricted to dim, fast-growing filaments, the sub-population whose growth is mediated by mDia1. Error bars indicate SE ($n \geq 20$).

Fig. S12

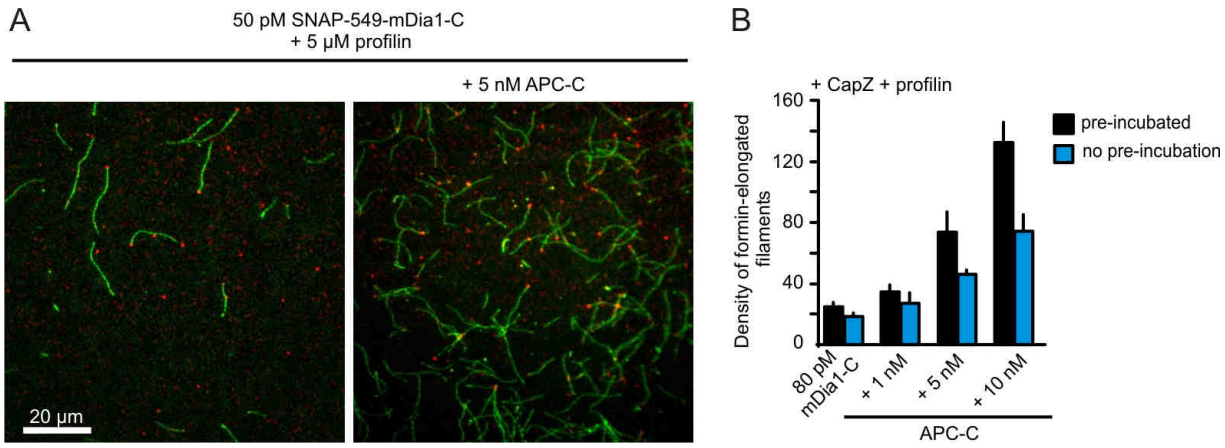

Fig. S12: Increase in the number of active formins by APC-C in presence of profilin. (A) Low magnification view; OG-actin filaments are green, SNAP-549-mDia1-C are red. (B) Number of formin-elongated filaments per 100 × 100 µm area for reactions containing 50 pM SNAP-549-mDia1-C, 1 nM CapZ, 5 µM profilin, and variable concentrations of APC-C. Error bars represent SD, *N*=3. mDia1-C and APC-C were either pre-incubated for 30 min (black bars) or not pre-incubated (blue bars). OG-actin (1 µM, 10% labeled) was added and the surface density of mDia1-formed filaments was measured by TIRFM (as in Figure 3B) after 5 min.

Fig. S13

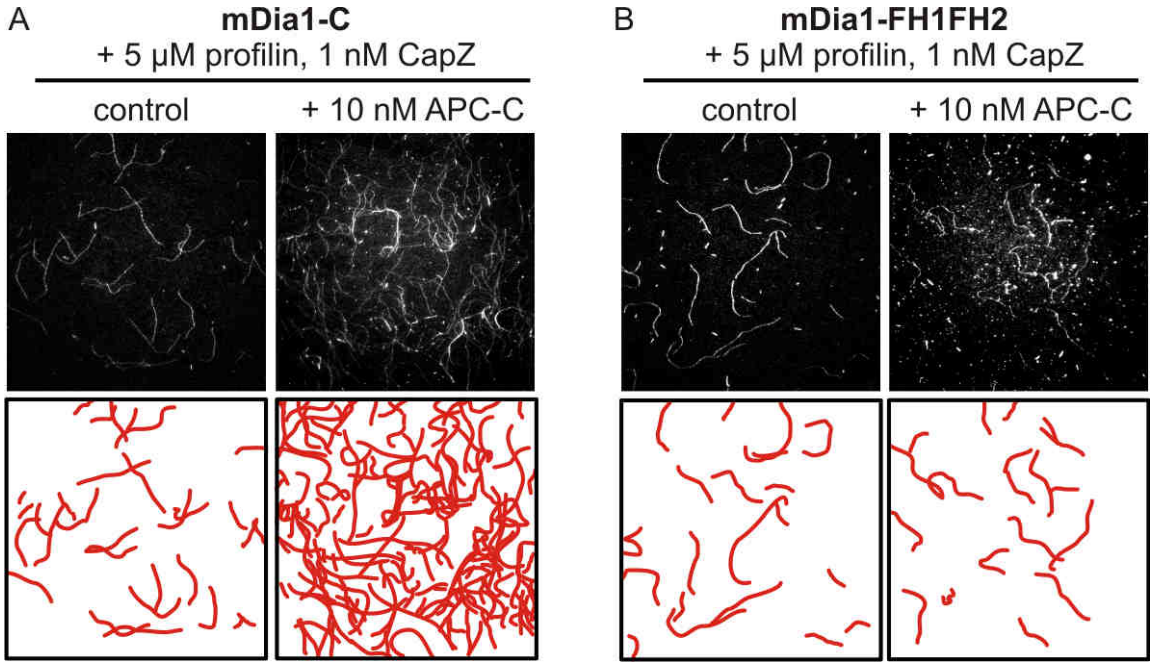

Fig. S13: Comparison of actin filament formation by mDia1-C versus mDia1-FH1FH2 in the presence and absence of APC-C. TIRFM images (top, each image 138 × 138 µm) and corresponding filament traces (bottom) for reactions containing 1 µM actin (10% OG-labeled), 80 pM formin, 5 µM profilin, 1 nM CapZ, ± 10 nM APC-C.

S**upporting movie legends**

Movie 1: Stepwise bleaching of SNAP-647-APC-C molecules. Surface adsorbed SNAP-647-APC-C molecules in 1X TIRF buffer in absence of glucose oxidase and catalase were bleached by continuous illumination. Red arrows indicate spots containing two, and yellow arrows indicate spots containing one fluorophore. Data are taken from the same experiment as Figure S1B. Each frame corresponds to 500 ms. The movie was speeded up 4-fold from real time.

Movie 2: Actin filament nucleation and filament-association of SNAP-647-APC-C. Dual-color TIRFM of OG-actin filaments (1 µM, 10% labeled, green) originating from SNAP-647-APC-spots (10 nM, red). Green arrowheads mark the growing barbed ends. The field of view corresponds to 33 × 36 µm. The movie represents a larger view of the micrographs shown in Figure 1A. Each frame corresponds to 3 s. The movie was speeded up 24-fold from real time.

Movie 3: Nucleation and bundling of multiple actin filaments by SNAP-647-APC-C. 1 µM OG-actin (green) was polymerized in the presence of 50 nM SNAP-647-APC-C (red), leading to the appearance of multiple filaments from APC clusters and concomitant filament bundling mediated by SNAP-647-APC-C binding along the side of the filament. The movie corresponds to Figure S3B. Each frame corresponds to 8 s. The movie was speeded up 64-fold from real time.

Movie 4: OG-actin accumulation in SNAP-647-APC-C spots in presence and absence of LatB. The movie shows the accumulation of OG-actin in SNAP-647-APC-C spots in absence (left) and presence (right) of LatB. In absence of LatB, formation of an actin filament occurs after ~60 seconds, while no filament assembly is observed in presence of LatB. The movies correspond to Figure 1C. Each frame corresponds to 3 s. The movie was speeded up 12-fold from real time.

Movie 5: Processive movement of SNAP-549-mDia1-C on a actin filament. 1 µM OG-actin (green) was polymerized in the presence of 50 pM SNAP-549-mDia1-C (red). The red arrow marks the processively moving formin. The movie corresponds to Figure 1D. Each frame corresponds to 10 s. The movie was speeded up 78-fold from real time.

Movie 6: Comparison of the elongation rates of free and formin-bound filament ends in the presence of profilin. 1 µM OG-actin was polymerized either alone (left) or in the presence of 100 pM mDia1-C (middle) or SNAP-549-mDia1-C (right, OG actin is green, SNAP-mDia1 is red) and 5 µM profilin. The right movie corresponds to Figure 1E. Each frame corresponds to 4 s. The movie was speeded up 24-fold from real time.

Movie 7: Evidence for processive filament elongation by single SNAP-549-mDia1-C molecules. 1 µM OG-actin (green) was polymerized in the presence of 50 pM SNAP-549-mDIa1-C (red) either in presence or absence of profilin. All movies correspond the micrographs shown in Figure S5A (+profilin) and B (-profilin). Each frame corresponds to 8 s (first movie), 6 s (second movie), 3 s (third movie) and 7 s (fourth movie) from left to right. The movies were speeded up 40-fold, 30-fold, 15-fold and 35-fold from real time, respectively.

Movie 8: Collaborative actin filament formation by SNAP-tagged mDia1-C and APC-C. Triple-color TIRFM of assembly of 1 µM OG-actin (green) in the presence of 50 pM SNAP-549-mDia1-C (red), 5 nM SNAP-647-APC-C (blue), 1 nM CapZ and 5 µM profilin. Arrows mark mDia1 (red) and APC (blue). The movie corresponds to Figure 3A. Each frame corresponds to 3 s. The movie was speeded up 27-fold from real time.

Movie 9: Collaborative actin filament formation by SNAP-tagged mDia1-C and APC-C in absence of profilin. Triple-color TIRFM of assembly of 1 µM OG-actin (green) in the presence of 50 pM SNAP-549-mDia1-C (red), 5 nM SNAP-647-APC-C (blue), and 1 nM CapZ. Arrows mark mDia1 (red) and APC (blue). The movie corresponds to Figure S5. Each frame corresponds to 10 s. The movie was speeded up 90-fold from real time.

References

1. T. D. Pollard, J. A. Cooper, Actin, a central player in cell shape and movement. *Science* **326**, 1208 (2009).

2. M. A. Chesarone, B. L. Goode, Actin nucleation and elongation factors: Mechanisms and interplay. *Curr. Opin. Cell Biol.* **21**, 28 (2009).

3. K. G. Campellone, M. D. Welch, A nucleator arms race: Cellular control of actin assembly. *Nat. Rev. Mol. Cell Biol.* **11**, 237 (2010).

4. M. E. Quinlan, S. Hilgert, A. Bedrossian, R. D. Mullins, E. Kerkhoff, Regulatory interactions between two actin nucleators, Spire and Cappuccino. *J. Cell Biol.* **179**, 117 (2007).

5. B. R. Graziano *et al*., Mechanism and cellular function of Bud6 as an actin nucleation-promoting factor. *Mol. Biol. Cell* **22**, 4016 (2011).

6. K. Okada *et al*., Adenomatous polyposis coli protein nucleates actin assembly and synergizes with the formin mDia1. *J. Cell Biol.* **189**, 1087 (2010).

7. A. Schirenbeck *et al*., The bundling activity of vasodilator-stimulated phosphoprotein is required for filopodium formation. *Proc. Natl. Acad. Sci. U.S.A.* **103**, 7694 (2006).

8. D. Pruyne *et al*., Role of formins in actin assembly: Nucleation and barbed-end association. *Science* **297**, 612 (2002).

9. H. Mizuno *et al*., Rotational movement of the formin mDia1 along the double helical strand of an actin filament. *Science* **331**, 80 (2011).

10. S. H. Zigmond *et al*., Formin leaky cap allows elongation in the presence of tight capping proteins. *Curr. Biol.* **13**, 1820 (2003).

11. D. R. Kovar, E. S. Harris, R. Mahaffy, H. N. Higgs, T. D. Pollard, Control of the assembly of ATP- and ADP-actin by formins and profilin. *Cell* **124**, 423 (2006).

12. M. A. Chesarone, A. G. DuPage, B. L. Goode, Unleashing formins to remodel the actin and microtubule cytoskeletons. *Nat. Rev. Mol. Cell Biol.* **11**, 62 (2010).

13. C. L. Vizcarra *et al*., Structure and function of the interacting domains of Spire and Fmn-family formins. *Proc. Natl. Acad. Sci. U.S.A.* **108**, 11884 (2011).

14. Materials and methods are available as supplementary material on *Science* Online.

15. J. B. Moseley *et al*., Regulated binding of adenomatous polyposis coli protein to actin. *J. Biol. Chem.* **282**, 12661 (2007).

16. Y. Wen *et al*., EB1 and APC bind to mDia to stabilize microtubules downstream of Rho and promote cell migration. *Nat. Cell Biol.* **6**, 820 (2004).

17. K. Zeth *et al*., Molecular basis of actin nucleation factor cooperativity: Crystal structure of the Spir-1 kinase non-catalytic C-lobe domain (KIND)•formin-2 formin SPIR interaction motif (FSI) complex. *J. Biol. Chem.* **286**, 30732 (2011).

18. B. M. McCartney, I. S. Näthke, Cell regulation by the Apc protein Apc as master regulator of epithelia. *Curr. Opin. Cell Biol.* **20**, 186 (2008).

19. T. Watanabe *et al*., Interaction with IQGAP1 links APC to Rac1, Cdc42, and actin filaments during cell polarization and migration. *Dev. Cell* **7**, 871 (2004).

20. Y. Mimori-Kiyosue, N. Shiina, S. Tsukita, Adenomatous polyposis coli (APC) protein moves along microtubules and concentrates at their growing ends in epithelial cells. *J. Cell Biol.* **148**, 505 (2000).

21. J. B. Moseley, S. Maiti, B. L. Goode, Formin proteins: Purification and measurement of effects on actin assembly. *Methods Enzymol.* **406**, 215 (2006).

22. C. J. Gould *et al*., The formin DAD domain plays dual roles in autoinhibition and actin nucleation. *Curr. Biol.* **21**, 384 (2011).

23. Y. Soeno, H. Abe, S. Kimura, K. Maruyama, T. Obinata, Generation of functional beta-actinin (CapZ) in an E. coli expression system. *J. Muscle Res. Cell Motil.* **19**, 639 (1998).

24. A. Keppler *et al*., A general method for the covalent labeling of fusion proteins with small molecules in vivo. *Nat. Biotechnol.* **21**, 86 (2003).

25. J. A. Spudich, S. Watt, The regulation of rabbit skeletal muscle contraction. I. Biochemical studies of the interaction of the tropomyosin-troponin complex with actin and the proteolytic fragments of myosin. *J. Biol. Chem.* **246**, 4866 (1971).

26. T. D. Pollard, J. A. Cooper, Quantitative analysis of the effect of Acanthamoeba profilin on actin filament nucleation and elongation. *Biochemistry* **23**, 6631 (1984).

27. J. B. Moseley *et al*., A conserved mechanism for Bni1- and mDia1-induced actin assembly and dual regulation of Bni1 by Bud6 and profilin. *Mol. Biol. Cell* **15**, 896 (2004).

28. J. R. Kuhn, T. D. Pollard, Real-time measurements of actin filament polymerization by total internal reflection fluorescence microscopy. *Biophys. J.* **88**, 1387 (2005).

29. D. Breitsprecher *et al*., Clustering of VASP actively drives processive, WH2 domain-mediated actin filament elongation. *EMBO J.* **27**, 2943 (2008).

30. D. R. Kovar, T. D. Pollard, Insertional assembly of actin filament barbed ends in association with formins produces piconewton forces. *Proc. Natl. Acad. Sci. U.S.A.* **101**, 14725 (2004).

31. N. Ramalingam *et al*., Phospholipids regulate localization and activity of mDia1 formin. *Eur. J. Cell Biol.* **89**, 723 (2010).